Macromolecules

Article

pubs.acs.org/Macromolecules

Comparison between Cellulose Nanocrystal and Cellulose Nanofibril Reinforced Poly(ethylene oxide) Nanofibers and Their Novel Shish-Kebab-Like Crystalline Structures

Xuezhu Xu,[†,‡] Haoran Wang,[†] Long Jiang,[†,*] Xinnan Wang,[†,‡] Scott A. Payne,[§] J. Y. Zhu,[∥] and Ruipeng Li[⊥]

[†]Department of Mechanical Engineering, [‡]Program of Materials and Nanotechnology, and [§]Electron Microscopy Core Facility, North Dakota State University, Fargo, North Dakota 58102, United States

[∥]USDA Forest Service, Forest Products Laboratory, Madison, Wisconsin 53726, United States

[⊥]CHESS/Wilson Lab, Cornell University, Ithaca, New York 14853, United States

ABSTRACT: Poly(ethylene oxide) (PEO) nanofiber mats were produced by electrospinning. Biobased cellulose nanocrystals (CNCs) and cellulose nanofibrils (CNFs) as reinforcement nanofillers were also added to the polymer to produce composite nanofiber mats. The effects of the two cellulose nanofillers on the rheological properties of the PEO solutions and the microstructure, crystallization, and mechanical properties of the mats were systematically compared. The microstructural disparity between the CNCs and CNFs led to significant differences in the solution viscosity, nanofiber morphology and microstructure of the composite nanofiber mats. A unique shish-kebab-like crystalline structure was discovered in both pure and filled PEO nanofibers. Both CNCs and CNFs showed strong reinforcing effects on the nanofiber mats.

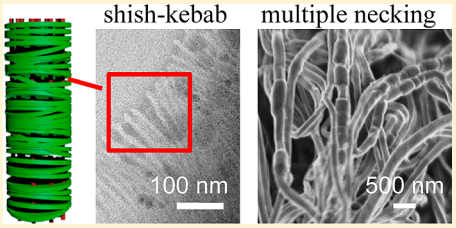

1. INTRODUCTION

The research on nanosized cellulose fibers has experienced an explosive growth in recent years because of the unique combination of their properties including outstanding mechanical properties, rich surface chemistry, nontoxicity, biocompatibility, and abundant renewable sources.[1−6] Cellulose nanocrystals (CNCs) and cellulose nanofibrils (CNFs) are the two types of cellulose nanofibers with very similar chemical compositions yet differing on morphologies due to their different manufacturing methods.[7,8] The CNCs are short, rod-like pure cellulose crystals whereas the CNFs are long, flexible, and entangled fibrils that readily gel in water and exhibit stronger reinforcing effect in polymer nanocomposites than the CNCs do.[9]

In polymer crystallization, highly oriented shish-kebab morphology, rather than conventional isotropic spherulitic morphology, is induced by flow.[10,11] The shishes consist of highly extended chains while the kebabs are lamellar crystals that grow epitaxially onto the shishes. Fibrillar fillers in polymer melts or solutions can also induce shish-kebab-like morphology during polymer crystallization without flow. In this case, the fillers, including inorganic whiskers, carbon nanotubes (CNTs), electrospun nanofibers, glass fibers and natural fibers, serve as the shishes and the crystalline polymers as the kebabs to form a hybrid structure.[12−15] Depending on the density of the nuclei on the filler surfaces and the geometry of the growing polymer crystals, different interfacial crystallization morphologies including hybrid shish-kebab, hybrid shish-calabash and trans-crystallization can be resulted.[16] The shish-kebab structures in pure polymers have been shown to lead to higher mechanical properties, decreased permeability, and improved thermal stability.[11] The interfacial crystallization in polymer/fiber composites has been found to be a highly effective way to enhance polymer/fiber interactions and hence to increase mechanical properties of the composites.[16]

Although the CNCs or CNFs have been utilized to reinforce electrospun polymer nanofibers in several studies,[17−22] the side-by-side comparisons in terms of their effects on rheological properties and spinnability of the electrospinning solutions, nanofiber diameter and diameter distribution, crystallization and mechanical properties of the nanofiber mats have not been attempted. In this study, electrospun PEO nanofiber mats with CNC or CNF reinforcement were prepared and their properties were systematically compared. An in-depth study on the crystalline structure of the nanofibers revealed a rarely seen shish-kebab-like structure.

2. EXPERIMENTAL SECTION

PEO powder (M_v = 1 000 000 g/mol) was purchased from Sigma-Aldrich. CNCs and CNFs (aqueous dispersions) were provided by the USDA Forest Service, Forest Products Laboratory (Madison, WI). The CNCs were produced by sulfuric acid hydrolysis, while the CNFs were produced through a multipass high-pressure grinding process using a Masuko MKZA6-2 Sangyo SuperMassColloider.[7,8] To prepare PEO/CNC and PEO/CNF dispersions, predetermined amounts of

Received: December 23, 2013
Revised: April 26, 2014
Published: May 12, 2014

the PEO powder, distilled water and the CNC or CNF aqueous dispersions were mixed to result in loadings of 0, 1, 4, 7, and 10 wt % of CNCs or CNFs (with respect to PEO weight). The PEO concentration was kept constant at 4 wt % for all the dispersions. Before electrospinning the dispersions were homogenized using an IKA T25 digital Ultra-Turrax homogenizer for 5 min (6000 rpm, room temperature) followed by magnetic stirring at ∼100 rpm at 60 °C for 12 h. The electrospinning was performed through a 25-gauge blunt needle under a flow rate of 0.1 mL/h. A 12 kV voltage was applied between the needle and the fiber collector (a spinning disc covered with aluminum foil) using a DC ES30 high voltage power supply (Gamma High Voltage Research). The collected nanofiber mats were kept in a desiccator before characterization.

A JEOL 7600 field-emission scanning electron microscopy (FE-SEM) operating at 2 kV was used to study nanofiber morphology. Small pieces of the nanofiber mat samples were cut from the aluminum foils and attached to the FE-SEM sample mounts using conductive carbon tapes. Prior to imaging, all samples were coated with a thin layer of carbon using a Cressington 208C carbon coater. The diameters of the nanofibers were determined based on the FE-SEM images using ImageJ software (National Institutes of Health, Bethesda, MD). One hundred total nanofibers for each sample were measured to obtain an average diameter. Transmission electron microscopy (TEM) imaging was performed using a JEOL JEM-2100 equipped with a LaB6 emitter. For CNC and CNF morphology, one droplet of CNC or CNF dispersion (diluted 100 times based on the as-received samples) was placed on a 300-mesh Formvar coated carbon film copper grid, air-dried and stained with 1% phosphotungstic acid. For the nanofibers, pure PEO, PEO/CNCs, or PEO/CNFs were electrospun onto the copper grids, stained by the phosphotungstic acid and imaged to study the dispersion of CNCs and CNFs. Some fibers were etched with water before staining.

Rheological properties of the electrospinning solutions were studied using a TA AR G2 rheometer equipped with φ 25 mm parallel plates. Steady shear tests were performed within the shear rate range of 0.01−100 s^{-1} using a gap size of 1 mm. Wide angle X-ray diffraction (WAXD) measurements were conducted using a Philips X'Pert MPD X-ray powder diffractometer with a Cu Kα X-ray source operating at 45 kV and 40 mA. Samples were scanned from 2.5 to 60° at 0.05°/s. Crystallite sizes were calculated using software MDI Jade 5.0 (Materials Data, Inc.).

Differential scanning calorimetry (DSC) tests were performed on a TA Q1000 equipment. For each sample, 2−6 mg of the material was tested in a hermetic aluminum pan under 50 mL/min nitrogen flow. The sample was heated to 100 °C at 10 °C/min, equilibrated at 100 °C for 2 min and cooled down to 20 °C at 10 °C/min. Tensile properties of the electrospun nanofiber mats were measured using a microtensile tester developed in our facility. The tester was equipped with a 5 lb LSM250 load cell (Futek Advanced Sensor Technology Inc.) and LabVIEW software (National Instruments) for test control and data acquisition. A tensile specimen (12.7 × 6.35 mm^2) was cut from a nanofiber mat and glued onto a card-paper frame. The frame was loaded onto the tester and the sides of the frame were clipped before the tension was applied. The specimens were stretched at a deformation rate of 7.62 mm/min. Nine repetitions were tested for each sample.

3. RESULTS AND DISCUSSION

3.1. Rheology of the PEO/CNC and PEO/CNF Dispersions. Nanoparticles show strong effects on the rheological properties of polymer solutions and melts because of their large surface areas. The effects of CNCs and CNFs on the rheology of PEO are expected to be different due to their different aspect ratios and microstructures as shown in Figure 1, parts a and a′. The entangled network structure of CNFs should cause higher viscosity of the PEO solutions. Steady shear viscosities of the pure PEO solution, as-received CNC and CNF dispersions, and PEO/CNC and PEO/CNF

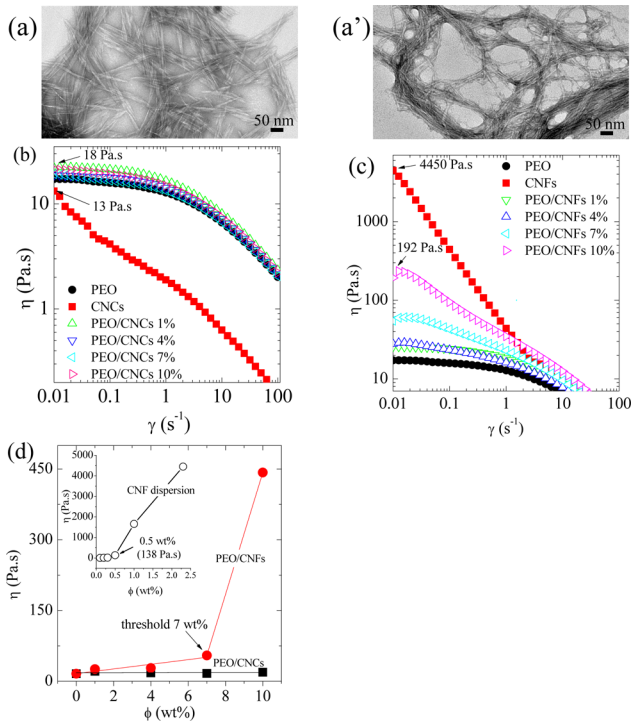

Figure 1. TEM images of needle-like CNCs (a) and network of CNFs (a′); (b) viscosity vs shear rate of the PEO/CNC dispersions; (c) viscosity vs shear rate of the PEO/CNF dispersions; (d) comparison of zero-shear viscosity between PEO/CNC and PEO/CNF dispersions. Inset: zero-shear viscosity of pure aqueous CNF dispersions.

dispersions are compared in Figure 1, parts b and c. The pure PEO solution exhibits a low-shear Newtonian region and a high-shear shear-thinning region, a typical rheological behavior of high molecular weight polymer solutions. The as-received CNC dispersion (5.7 wt %) shows the lowest zero shear viscosity (13 Pa·s) among all the tested samples because of the lack of interparticle interactions (i.e., no network structure) at such low CNC concentration. The dispersion also exhibits strong shear thinning behavior over the whole shear rate range due to progressive CNC alignment in the flow direction. Viscosities of the PEO/CNC dispersions are only slightly higher than that of the pure PEO solution, indicating the lack of interparticle interaction and that the increase in viscosity is largely due to a hydrodynamic effect (Figure 1b). By contrast, the as-received CNF dispersion (2.3 wt %) shows the highest zero shear viscosity (4450 Pa·s) and the strongest shear thinning behavior among all the tested samples (Figure 1c), which is ascribed to the network structure of CNFs and its progressive disruption under shearing.[23] Viscosities of the PEO/CNF dispersions are also much higher than those of the comparable PEO/CNC dispersions because of the entanglements between individual CNFs. Figure 1d compares the zero shear viscosities of the two dispersions over 0−10 wt % loading range. While the viscosities of PEO/CNCs remain nearly constant, the viscosities of PEO/CNFs show a rapid increase above 7 wt % CNFs (corresponding to 0.28 wt % CNFs with respect to water), which appears to indicate the formation of a percolated CNF network structure in the PEO/CNF dispersions. For comparison, the zero shear viscosities of pure CNF aqueous dispersions containing different concentrations of CNFs were also measured and the results are shown in

dx.doi.org/10.1021/ma402627j | Macromolecules 2014, 47, 3409−3416

Figure 1d inset. The results indicate a CNF percolation concentration of 0.5 wt %. This higher percolation threshold suggests that PEO chains in the PEO/CNF dispersions facilitate CNF percolation, possibly by bridging CNFs through the strong interactions between the two components.[9] The percolation of the CNFs tends to clog the needle during electrospinning and hence to interrupt the process, as will be discussed later.

3.2. Morphology of Electrospun Nanofibers. Parts a–d of Figure 2 show the surface morphologies of the PEO/CNC and PEO/CNF nanofibers. Both nanofibers exhibit smooth surfaces without any sign of surface coarsening due to the addition of the nanosized cellulose fibers, suggesting homogeneous dispersion of the cellulose fibers in the PEO matrix, which is facilitated by the hydrogen bonding between them.[9] It is worth noting that above 10 wt % CNF concentration, the electrospinning process of the PEO/CNF dispersion was frequently interrupted by the ejection of large droplets from the needle due to the high viscosity of the dispersion and/or CNF flocculation induced phase separation in the dispersion.[19] The PEO/CNC dispersions, on the other hand, could be successfully electrospun into homogeneous nanofibers up to 20 wt % CNC concentration because of the lack of CNC flocculation.

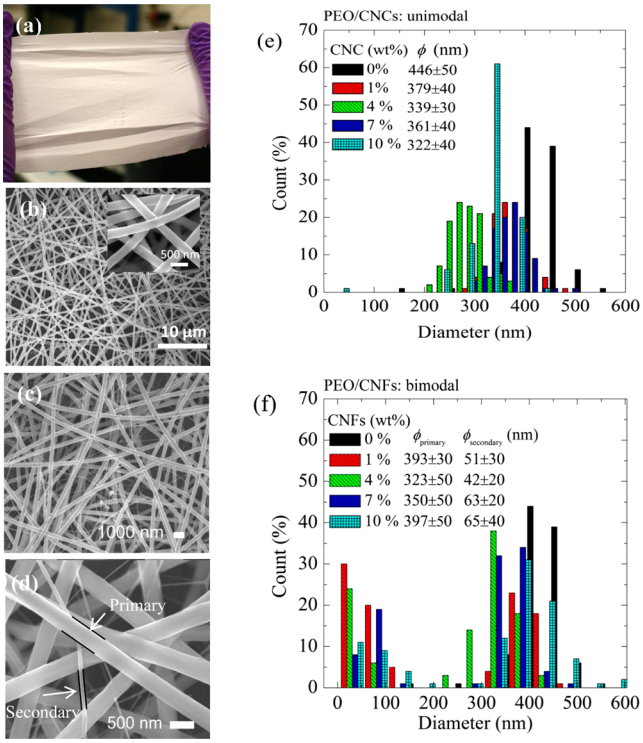

Figure 2. . Photo (a) and FE-SEM micrograph (b) of PEO/CNC 1% nanofiber mat; (c, d) FE-SEM images of PEO/CNF 1% nanofiber mat; (e) diameter distribution of the PEO/CNC nanofibers; (f) diameter distribution of PEO/CNF nanofibers.

The diameter histogram of the PEO/CNC nanofibers and the average diameter (ϕ) for each fiber are shown in Figure 2e. All the fibers exhibit a unimodal size distribution and the average diameter decreases with increasing CNC concentration. The decrease can be ascribed to the increased conductivity of the dispersions that results in larger electrostatic pulling force on the jets.[24−27] In contrast, all the PEO/CNF nanofibers exhibit a bimodal size distribution as shown in Figure 2f. Basically, during the electrospinning, a primary jet splits into multiple secondary jets once the electrical charge-induced radial repulsive force exceeds the cohesive force of the jet.[28] The bimodal diameter distribution may be due to the uneven distribution of the charges induced by the highly entangled network structure of CNFs, which leads to uneven splitting of the jet when subjected to the electric field.[29] This phenomenon has also been frequently reported in other highly viscous liquids with the electrical instability by other investigators.[30,31]

3.3. PEO Crystallization in the Electrospun Nanofibers. Figure 3a shows a TEM micrograph of the pure PEO nanofiber. A shish-kebab-like crystal stucture can be clearly seen. The "kebabs" are perpendicular to the fiber axis and are peroidically located along the fiber. Such configuration of crystal structure is rarely seen in electrospun nanofibers. Wang et al. have reported PEO nano hybrid shish-kebab (NHSK) structure, where PEO kebabs grow on electrospun PEO nanofibers in a controlled solution crystallizaztion process.[32] The TEM micrograph of this NHSK stucture appears similar to Figure 3a. However, the origins of the kebabs in the two studies are totally different: the "kebabs" in this study are formed inside the electrospun nanofiber whereas in Wang's study the kebabs crystallize onto the nanofiber surfaces in a secondary crystallization process. The "kebabs" in this study exhibit an average thickness of 11 nm and a period of 9−25 nm. The period is much smaller than that of the NHSK kebabs[13] and classic polymer shish-kebabs formed under flow.[12]

The shish-kebab-like crystal stuctures also exist in PEO/CNC and PEO/CNF nanofibers as shown in Figure 3b. A brief water etching process on the nanofiber led to a shish-kebab-like PEO crystal structure (Figure 3c) similar to that of electrospun polyethylene (PE) nanofibers, where extended PE shishes and perpendicular kebabs were clearly identified.[33] The selected area electron diffraction (SAED) pattern (Figure 3d) taken from Figure 3b exhibits characteristic (120) diffraction that suggests unidirectional orientation of the PEO chains in the fiber direction.[32,34] Long time water etching dissoved all PEO and only the cellulose nanofillers remained. The nanofillers appear to be largely aligned in the axial direction of the fiber due to the jet stretching during electrospinning[19] (Figure 3e,f). Regarding the formation mechanism of the shish-kebab-like structures in the pure PEO nanofibers, some PEO chains were first oriented in the axial direction by the stretching force and possibly formed extended chain crystals.[32] The remaining crystallizable PEO chains crystallized epitaxally or soft-epitaxally on the extended chains to form the "kebabs". For the PEO/CNC or PEO/CNF nanofibers, the cellulose nanofillers could also serve as the "shishes" to facilitate the growth of PEO "kebabs".[35] A schematic illustration of such shish-kebab-like structure is shown in Figure 3g.

WAXD was used to determine PEO crystal structures in the nanofibers. The diffraction patterns and the derived crystal characteristics including 2θ, d-spacing and average crystallite size (L) are given in Figure 3h and Table 1, respectively. The crystallite size was calculated based on the Scherrer's equation:

$$L = K\lambda/B \cos\theta$$

where K is the Scherrer constant (0.89), λ is the wavelength of the Cu Kα X-ray (1.54 Å), and B is the full width at half-maximum (fwhm) of diffraction peaks. The pure PEO nanofibers exhibit two strong peaks at 19° and 23°, which are attributed to the diffraction of the (120) and (112) crystal

dx.doi.org/10.1021/ma402627j | Macromolecules 2014, 47, 3409−3416

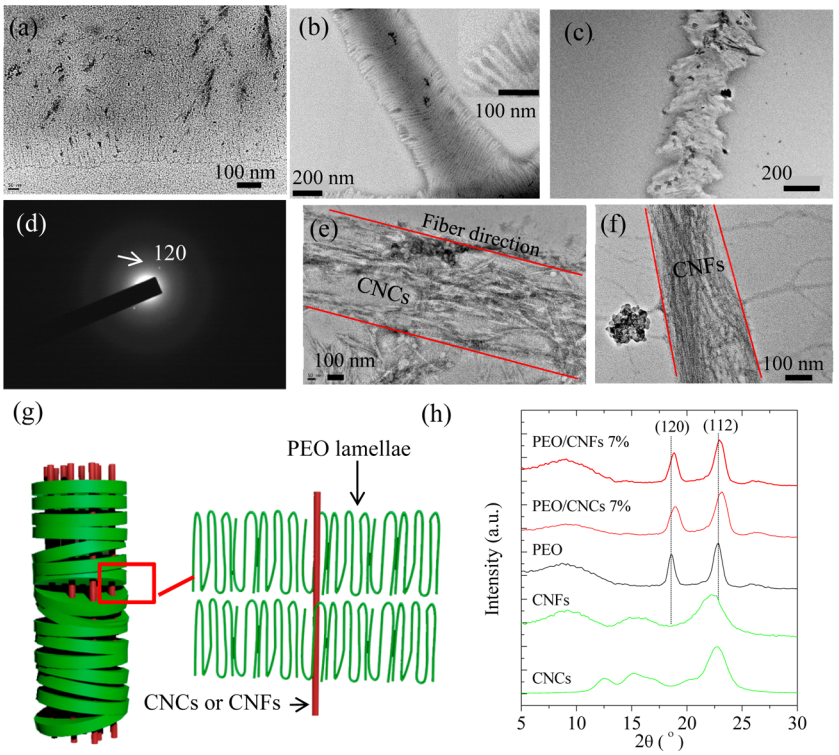

Figure 3. (a) TEM images of pure PEO nanofibers; (b) PEO/CNF 4% nanofibers; (c) PEO/CNF 4% nanofiber after mild water etching; (d) SAED pattern taken from Figure b; (e) PEO/CNC 4% and (f) PEO/CNF 4% nanofibers after PEO removal; (g) illustration of the shish-kebab-like structure; (h) WAXD patterns of PEO/CNC and PEO/CNF 7% nanofibers.

Table 1. XRD Results of the Pure PEO, PEO/CNC (7 wt %), and PEO/CNF (7 wt %) Nanofibers

	(120)				(112)			
sample	2θ (deg)	d-spacing (Å)	fwhm	L (Å)	2θ (deg)	d-spacing (Å)	fwhm	L (Å)
PEO	18.6	4.8	0.614	157	22.8	3.9	0.769	106
PEO/CNCs	18.9	4.7	0.805	96	23.1	3.8	0.997	88
PEO/CNFs	18.8	4.7	0.676	110	22.9	3.9	0.789	94

planes.[26] The CNCs and CNFs feature typical diffraction peaks of cellulose I and II.[9] The (120) and (112) diffraction peaks are broadened and shifted to higher angles when CNCs or CNFs are incorporated into the nanofibers, suggesting reduced d-spacing and crystallite size. As shown in Table 1, the d-spacings for both PEO/CNCs and PEO/CNFs show slight decreases whereas the crystallite sizes exhibit substantial decreases. For example, pure PEO exhibits crystal sizes of 157 and 106 Å at (120) and (112) planes respectively, whereas PEO/CNF 7 wt % possesses comparable sizes of 110 and 94 Å. The sizes are reduced by 4.7 and 1.2 nm in the two directions.

3.4. Thermal Properties of PEO/CNC and PEO/CNF Nanofibers. The effects of the CNCs and CNFs on the melting and crystallization of PEO nanofibers were studied using DSC. Pure PEO powder and pure electrospun PEO nanofiber were also tested for comparisons. In Figures 4, the pure PEO powder exhibits one single melting peak at 68.4 °C whereas the pure nanofiber exhibits a broad melting region which can be separated into a low (66.3 °C) and a high (71.9 °C) melting peak. Double-melting peak has been reported on electrospun nanofibers[36,37] and polymers having high degree of shear-induced chain orientation.[38] It can indicate the coexistence of two different crystalline types: lamellar crystals (low melting point) and extended chain crystals (high melting point) in the pure PEO nanofibers. The melting point of the lamellae in the electrospun nanofiber is even lower than that of the regular lamellae in the PEO powder because of rapid solidification of the fiber during electrospinning. The electrospun nanofibers containing CNCs or CNFs also exhibit broadened double melting peaks, indicating similar coexistence of nonoriented and oriented crystals. However, at 10% CNCs or CNFs, the double melting is substantially suppressed because high concentration of nanoparticles hinders the growth of PEO lamellae.[39]

The melting point (T_m), heat of fusion (ΔH), and crystallinity (X_c) of the samples were derived from the DSC thermograms and their results are summarized in Table 2. The crystallinity of the PEO nanofibers is substantially lower than that of the PEO powder (73% vs 90%) due to the rapid solidification of nanofibers, which restricts crystal growth. The nucleation effects of CNCs and CNFs increase the crystallinity of PEO/CNC and PEO/CNF nanofibers at low filler concentrations. However, at high concentrations, the diffusion of PEO chains and hence the growth of the lamellae are hindered and as a result, the crystallinity starts to decrease. The nucleation effects of CNCs and CNFs are also demonstrated by the cooling thermograms in Figure 4, parts c and d. The crystallization peaks of PEO are shifted to higher temperatures when CNCs or CNFs are added, and then the peak temperature (T_c) in general decreases with increasing nanofiller

dx.doi.org/10.1021/ma402627j | Macromolecules 2014, 47, 3409−3416

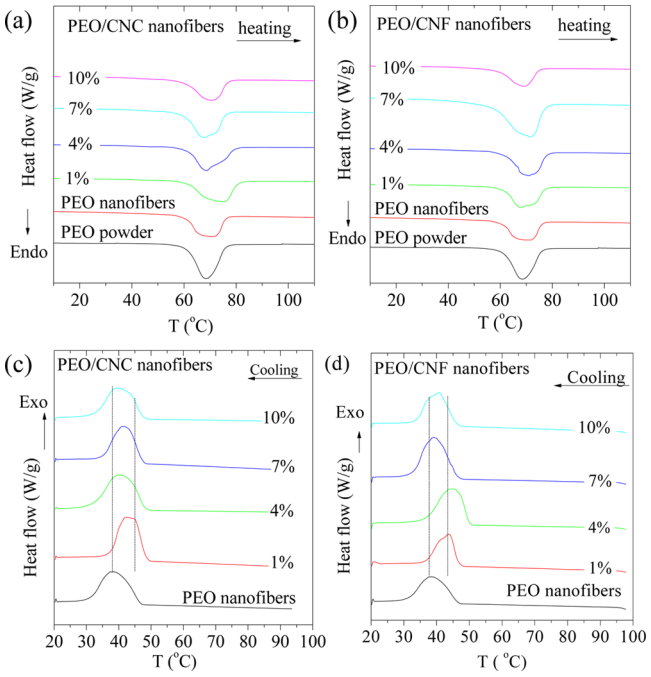

Figure 4. DSC thermograms for the melting and nonisothermal crystallization of PEO/CNC and PEO/CNF nanofibers: (a) PEO/CNC melting; (b) PEO/CNF melting; (c) PEO/CNC crystallization; (d) PEO/CNF crystallization.

concentrations due to suppressed crystal growth. The largest increases in the T_c and T_o (onset temperature) are 6.3 and 3.5 °C, respectively, which both occur on the 4% PEO/CNF nanofibers.

It is also worth noting from Table 2 that melting temperatures of PEO/CNCs are generally higher than those of PEO/CNFs. We postulate that this is due to higher perfection of the shish-kebab-like structure in the former. CNCs can be aligned during electrospinning more readily than CNFs because of the following two reasons: CNCs are rigid rods without entanglements and PEO/CNC solutions exhibit lower viscosities than PEO/CNF solutions. Both reasons lead to lower resistance to CNC rotation and therefore higher degree of CNC alignment, which facilitates the formation of PEO "shish kebab". In addition, the lower viscosity of the PEO/CNC solutions allows PEO chains to diffuse at a higher rate to the growing fronts of the "kebabs", promoting growth of the structure.

Comparing the melting points of the nanofiber mats to those of the cast films in our previous study,[9] it is obvious that the melting points of the former are generally increased by the cellulose nanofibers (especially at low CNC or CNF concentrations), whereas the melting points are decreased by the nanofibers in the latter due to the nanofiber confinement effect which hinders chain diffusion and folding. This comparison shows that the formation of the shish-kebab-like structures, which is facilitated by the extensional flow generated by electrospinning and CNC (or CNF) assisted PEO chain alignment and crystallization, dominates the crystallization process of the nanofiber mats.

3.5. Mechanical Properties of Nanofiber Mats.

Representative tensile stress−strain curves of the PEO/CNC and PEO/CNF nanofiber mats and their FE-SEM micrographs after tensile fracture are shown in Figure 5. The Young's modulus, tensile strength, strain-at-failure and toughness of the samples are summarized in Table 3. For the CNC reinforced nanofiber mats, all the measured properties peak at 1 wt % filler concentration and then continuously decrease with the increasing concentration. The tensile strength and Young's modulus for the 1 wt % mat are 2.2 and 3.5 times as large as those of the pure PEO membrane. Strain-at-failure and fracture toughness at the same time increase to 1.3 and 3 times the control values. For the CNF reinforced mats, the maximum values of all the properties occur at 4 wt % CNF concentration. At this concentration, the strength, modulus, strain and toughness are 2.5, 1.4, 1.3, and 2.2 times the control values, respectively. For both types of mats, at the 10 wt % highest concentration, the strength and modulus of the mats are still comparable to the control values, if not higher. However, the strain and toughness are significantly lower (less than half), indicating increased brittleness of the mats after incorporating high concentrations of the cellulose nanofillers. No direct correlations can be found between fiber diameter and the mechanical properties for both PEO/CNC and PEO/CNF nanofiber mats. More discussion on this is given below.

Failure mechanisms of the PEO/CNC and PEO/CNF nanofiber mats were studied based on the SEM micrographs of the fractured mats. Multinecking can be clearly seen from the pure PEO nanofibers (Figure 5c). This phenomenon has also been reported on electrospun carbon nanotube (CNT) reinforced polymer nanofibers.[40−42] In polymer deformation, necking refers to localized large scale plastic deformation initiated by material defects (voids, cracks, etc.) and inclusions (nanofibers, particles, etc.) which cause stress concentration.

Table 2. DSC Results for the Electrospun Nanofibers

	sample	0%	1%	4%	7%	10%
T_m (°C)	PEO/CNCs	66.3, 71.9	68.7, 75.6	68.2, 75.6	68.0, 72.1	70.2
	PEO/CNFs		67.2, 73.3	67.6, 73.3	70.2	68.7
ΔH (J/g)	PEO/CNCs	157	183.8	181.3	179.2	177.3
	PEO/CNFs		167.1	161.1	164.6	154.8
X_c (%)[a]	PEO/CNCs	73	87	88	81	79
	PEO/CNFs		79	80	83	80
T_0 (°C)	PEO/CNCs	46.4	48.3	48.1	47.3	47.3
	PEO/CNFs		46.4	49.9	46.4	46.3
T_c (°C)	PEO/CNCs	38.6	43.0	40.3	41.8	39.7
	PEO/CNFs		44.0	44.9	39.3	40.8

[a] $X_c = \Delta H/[\Delta H_{100\%} \times (1 - W)]$,where $\Delta H_{100\%}$ is the heat of fusion for 100% crystallized PEO (213.7 J/g).[34] W is the weight fraction of CNCs or CNFs. The T_m, ΔH, and X_c for PEO powder was 68.4 °C, 192.1 J/g, and 90%, respectively.

dx.doi.org/10.1021/ma402627j | Macromolecules 2014, 47, 3409−3416

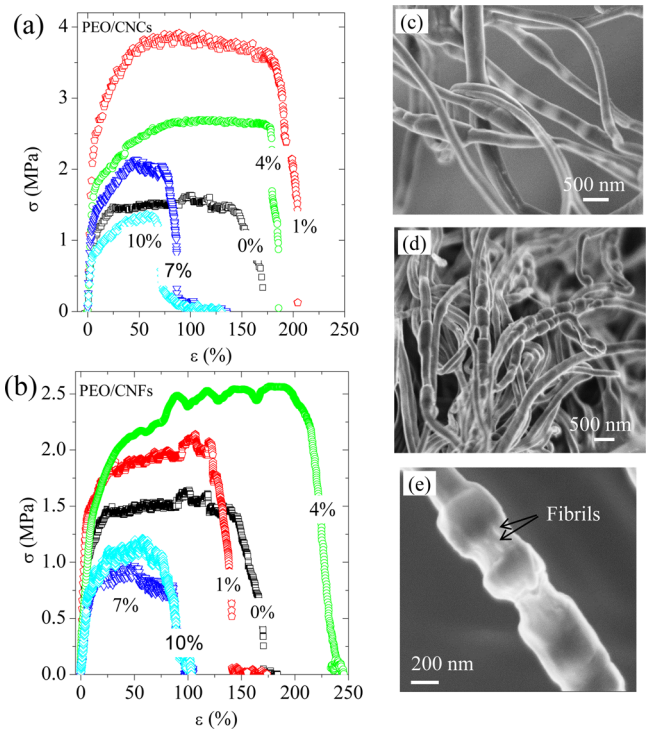

Figure 5. Stress–strain curves of PEO/CNC (a) and PEO/CNF (b) nanofiber mats with various filler contents; (c) FE-SEM images of pure PEO nanofiber membrane after testing; (d) 1 wt % PEO/CNC nanofiber membrane after testing; (e) fibrillation in the neck region of the PEO/CNF 4% fiber.

Table 3. Mechanical Properties of PEO/CNC and PEO/CNF Nanofiber Mats

filler	filler content (wt %)	Young's modulus (MPa)	tensile strength (MPa)	strain-at-failure (%)	fracture toughness (kJ/m^3)
PEO	0	20 ± 1	1.6 ± 0.2	152 ± 31	232 ± 20
CNCs	1	72 ± 20	3.5 ± 0.6	204 ± 30	702 ± 45
	4	56 ± 20	2.9 ± 0.4	185 ± 11	448 ± 16
	7	50 ± 10	1.9 ± 0.2	87 ± 12	153 ± 11
	10	22 ± 3	1.3 ± 0.2	71 ± 7	84 ± 3
CNFs	1	44 ± 9	2.1 ± 0.1	119 ± 25	400 ± 40
	4	51 ± 10	2.2 ± 0.3	197 ± 10	513 ± 16
	7	24 ± 10	0.8 ± 0.2	86 ± 18	72 ± 22
	10	20 ± 3	1.2 ± 0.3	75 ± 12	86 ± 9

During the necking process, the material in the neck is cold-drawn and the cross-sectional area is reduced. The polymer chains in the neck are aligned in the stretching direction and the material is strain hardened. The degree of necking is characterized by the draw ratio that can be defined as the diameter of the fiber out of the neck region divided by that in the neck region. A large draw ratio and high-frequency multinecking lead to large strain-at-failure and fracture toughness of the material. The pure PEO nanofibers (Figure 5c) exhibit a relatively small average draw ratio of 1.27, whereas the ratios for the PEO/CNC (1 wt %) and PEO/CNF (4 wt %) nanofibers increase to 2.49 and 1.64, respectively, matching the increasing trend of the strain-at-failure and fracture toughness. Moreover, the frequency of necking also appears to increase in the CNC or CNF filled nanofibers (Figure 5d) because of the additional stress concentration sites caused by the nanofillers.[42]

The fibrils formed after crazing can be clearly seen in the neck region of the nanofibers (Figure 5e). Ye et al. reported the similar phenomenon in stretched electrospun CNT-polyacrylonitrile nanofibers and proposed a two-stage deformation mechanism including crazing and fiber pull-out in the neck region.[41] In our study, CNCs and CNFs at their low concentrations promote and stabilize multinecking and hence increase the failure strain and toughness. The nanofillers in the neck region, being largely aligned in the longitudinal direction by the stretching and by the prior electrospinning process, share the load from the PEO matrix and hinder rapid craze propagation in the matrix, thus causing the increase in the strength of the nanofibers.[41,42] The crazing fibrils shown in Figure 5e contains CNCs or CNFs and their encapsulating PEO sheath. Due to the strong hydrogen bonding between the nanofillers and PEO, we postulate that no CNC or CNF fiber pull-out occurs in this system. Rather, the PEO molecules around the nanofillers slip and align by shearing along the nanofillers, leading to the fibrillar structure shown in Figure 5e.[42]

The continuous decreases of all the mechanical properties at high CNC (>1 wt %) or CNF (>4 wt %) concentrations are believed to be mainly caused by nanofiller agglomeration, which is likely to occur during fiber solidification after it is ejected out of the needle. Instead of facilitating crazing, large nanofiller agglomerates lead to cracks that propagate readily in the nanofibers and result in premature fiber fractures. The reason for the higher transition concentration of CNFs is unclear. It may be related to the bimodal distribution of the PEO/CNF nanofibers, which leads to microstructural disparities between the PEO/CNF and PEO/CNC nanofiber mats. It should be pointed out that in this study nonwoven fiber mats rather than single fiber or unidirectional fiber mats was used for the tensile tests. As a result, the mechanical properties obtained from the tests (Table 3) do not directly represent those of single nanofibers. Pai et al. developed a quantitative microstructure-based model that relates the moduli of electrospun nanofiber mats to those of the individual nanofibers.[43] The model indicates that the moduli of the mats is a function of the moduli of the individual nanofibers, porosities of the mats, fiber diameters, junction lengths, and radii of curvature of the nanofibers. The last two parameters are further shown to be proportional to the fiber diameter. A larger diameter causes higher junction length and radius of curvature, which in turn leads to an increase in the modulus of the nanofiber mats. However, the increase can be offset by the decrease in intrinsic nanofiber modulus, which is attributed to reduced chain orientation. As a result, the moduli and strengths of poly(trimethyl hexamethylene terephthalamide) model mats remain largely constant with increasing nanofiber diameter (113–3643 nm).

The above-mentioned study sheds light on the mechanical properties of the nanofiber mats in this research. All the PEO/CNF nanofiber mats exhibit similar fiber diameter and diameter distribution regardless of their CNF contents. Their porosities have also been found similar (0.79 ± 0.04) based on the densities of the mats and the densities of PEO/CNF cast films (Pai has also shown nearly constant mat porosity (0.88–0.90) for a fiber diameter range of 113–3643 nm).[43] Due to the consistency in fiber diameter and in mat porosity across the PEO/CNF mats, the substantial variations in their mechanical properties (Table 3) can only be caused by the changes in the intrinsic properties of the individual nanofibers, which vary

dx.doi.org/10.1021/ma402627j | Macromolecules 2014, 47, 3409–3416

according to the concentration of CNFs. As for the PEO/CNC nanofiber mats, their porosity also remains relatively constant (0.85 ± 0.03). Although the fiber diameter decreases moderately with increasing CNC concentration, the diameter change alone should not cause large variations in the strength and modulus of the mats base on the results of Pai.[43] Therefore, the variations that do occur on PEO/CNC nanofiber mats (Table 3) is due to the mechanical property changes of individual PEO/CNC nanofibers. In conclusion, the increases in mechanical properties of the nanofiber mats are primarily caused by the reinforcing effects of CNCs or CNFs on the individual nanofibers, with the microstructural effects of the fiber mats being relatively small.

In addition to the reinforcing effects of CNCs and CNFs, the effects of PEO crystallinity and crystal size on the mechanical properties of the nanofibers should not be ignored. Our DSC results show that PEO crystallinity is higher in the samples containing CNCs or CNFs while the WAXD results indicate that the size of PEO crystals is smaller. This means that CNCs and CNFs lead to higher density but smaller PEO crystals in the nanofibers. Mechanical properties of a semicrystalline polymer such as PEO can be simulated using composite mechanics—a rigid crystalline phase dispersed in a relatively soft amorphous matrix as reinforcement.[44] On the basis of the composite theory, modulus of the semicrystalline polymer increases with the fraction of the rigid crystalline phase.[45] Strength of the composite can also be increased if there is a strong interfacial bonding between the two phases, which is often the case for semicrystalline polymers because of the existence of tie chains that connect the crystalline and amorphous phases. Smaller crystals means larger interfacial area between the two phases (assuming equal crystallinity) and less stress concentration, both of which positively contribute to the strength of the semicrystalline polymer. Therefore, the increased crystallinity and reduced crystal size of the PEO/CNC and PEO/CNF nanofibers as well as the reinforcement of CNCs (or CNFs) contribute synergistically to the increases in mechanical properties of the nanofiber mats at low CNC (or CNF) concentrations. At high concentrations, CNC (or CNF) agglomeration dominates the above factors and causes decreases in mechanical properties of the nanofiber mats.

4. CONCLUSIONS

CNCs and CNFs were used as reinforcement materials in electrospun PEO nanofiber mats and their effects on the viscosity of the spinning solutions, nanofiber diameter and diameter distribution, crystalline structures of the nanofibers, and the mechanical properties of the nanofiber mats were systematically studied. The CNFs caused high viscosity of the PEO solutions, relatively poor spinnability and bimodal fiber diameter distribution due to their entangled network structure. Rare shish-kebab-like PEO crystalline structures were discovered in the electrospun nanofibers. Mechanical properties of the nanofiber mats, including strength, modulus and fracture toughness, were significantly improved by the addition of low concentrations of CNCs and CNFs. The properties deteriorated at high concentrations of the nanofillers due to filler agglomeration.

AUTHOR INFORMATION

Corresponding Author

*(L.J.) E-mail: long.jiang@ndsu.edu. Telephone: +1 (701) 231 9512. Fax: +1 (701) 231 8913.

Notes

The authors declare no competing financial interest.

ACKNOWLEDGMENTS

Financial supports from North Dakota EPSCoR and US Forest Service are greatly appreciated. Ms. Chenguang Long from Industrial and Manufacturing Engineering Department of NDSU is appreciated for conducting some of the experiments.

REFERENCES

(1) Habibi, Y.; Lucia, L. A.; Rojas, O. J. *Chem. Rev.* **2010**, *110*, 3479.
(2) Peng, B. L.; Dhar, N.; Liu, H. L.; Tam, K. C. *Can. J. Chem. Eng.* **2011**, *89*, 1191.
(3) Siró, I.; Plackett, D. *Cellulose* **2010**, *17*, 459.
(4) Dufresne, A. *Can. J. Chem.* **2008**, *86*, 484.
(5) Eichhorn, S. J.; Dufresne, A.; Aranguren, M.; Marcovich, N. E.; Capadona, J. R.; Rowan, S. J.; Weder, C.; Thielemans, W.; Roman, M.; Renneckar, S.; Gindl, W.; Veigel, S.; Keckes, J.; Yano, H.; Abe, K.; Nogi, M.; Nakagaito, A. N.; Mangalam, A.; Simonsen, J.; Benight, A. S.; Bismarck, A.; Berglund, L. A.; Peijs, T. *J. Mater. Sci.* **2009**, *45*, 1.
(6) Durán, N.; Lemes, A. P.; Seabra, A. B. *Recent Pat. Nanotechnol.* **2012**, *6*, 16.
(7) Wang, Q. Q.; Zhu, J. Y.; Gleisner, R.; Kuster, T. A.; Baxa, U.; McNeil, S. E. *Cellulose* **2012**, *19*, 1631.
(8) Wang, Q. Q.; Zhu, J. Y.; Reiner, R. S.; Verrill, S. P.; Baxa, U.; McNeil, S. E. *Cellulose* **2012**, *19*, 2033.
(9) Xu, X.; Liu, F.; Jiang, L.; Zhu, J. *ACS Appl. Mater. Interfaces* **2013**, *5*, 2999.
(10) Somani, R. H.; Yang, L.; Zhu, L.; Hsiao, B. S. *Polymer* **2005**, *46*, 8587.
(11) Wang, K.; Chen, F.; Zhang, Q.; Fu, Q. *Polymer* **2008**, *49*, 4745.
(12) Yang, J.; Wang, C.; Wang, K.; Zhang, Q.; Chen, F.; Du, R.; Fu, Q. *Macromolecules* **2009**, *42*, 7016.
(13) Ning, N.; Luo, F.; Pan, B.; Zhang, Q.; Wang, K.; Fu, Q. *Macromolecules* **2007**, *40*, 8533.
(14) Dufresne, A.; Kellerhals, M. B.; Witholt, B. *Macromolecules* **1999**, *32*, 7396.
(15) Zhong, G. J.; Li, Z. M.; Li, L.; Shen, K. *Polymer* **2008**, *49*, 4271.
(16) Ning, N.; Fu, S.; Zhang, W.; Chen, F.; Wang, K.; Deng, H.; Zhang, Q.; Fu, Q. *Prog. Polym. Sci.* **2012**, *37*, 1425.
(17) Li, Y.; Ko, F. K.; Hamad, W. Y. *Biomacromolecules* **2013**, *14*, 3801.
(18) Fortunato, G.; Zimmermann, T.; Lübben, J.; Bordeanu, N.; Hufenus, R. *Macromol. Mater. Eng.* **2012**, *297*, 576.
(19) Olsson, R. T.; Kraemer, R.; López-Rubio, A.; Torres-Giner, S.; Ocio, M. J.; Lagarón, J. M. *Macromolecules* **2010**, *43*, 4201.
(20) Medeiros, E. S.; Mattoso, L. H. C.; Ito, E. N.; Gregorski, K. S.; Robertson, G. H.; Offeman, R. D.; Wood, D. F.; Orts, W. J.; Imam, S. H. *J. Biobased Mater. Bio.* **2008**, *2*, 231.
(21) Park, W.; Kang, M.; Kim, H. S.; Jin, H. J. *Macromol. Symp.* **2007**, *249−250* (1), 289.
(22) Changsarn, S.; Mendez, J. D.; Shanmuganathan, K.; Foster, E. J.; Weder, C.; Supaphol, P. *Macromol. Rapid Commun.* **2011**, *32* (17), 1367.
(23) Liu, D.; Chen, X.; Yue, Y.; Chen, M.; Wu, Q. Structure and Rheology of Nanocrystalline Cellulose. *Carbohyd. Polym.* **2011**, *84*, 316.
(24) Yarin, A. L.; Koombhongse, S.; Reneker, D. H. *J. Appl. Phys.* **2001**, *89*, 3018.
(25) Reneker, D. H.; Yarin, A. L.; Fong, H.; Koombhongse, S. *J. Appl. Phys.* **2000**, *87*, 4531.
(26) Zhou, C.; Chu, R.; Wu, R.; Wu, Q. *Biomacromolecules* **2011**, *12*, 2617.
(27) Demir, M. M.; Yilgor, I.; Yilgor, E.; Erman, B. *Polymer* **2002**, *43*, 3303.
(28) Reneker, D. H.; Chun, I. *Nanotechnol.* **1996**, *7*, 216.
(29) Hsu, C. M.; Shivkumar, S. *Macromol. Mater. Eng.* **2004**, *289*, 334.

(30) Hsu, C. M.; Shivkumar, S. *J. Materi. Sci.* **2004**, *39*, 3003.
(31) Ku, B. K.; Kim, S. S. *J. Aerosol Sci.* **2002**, *33*, 1361.
(32) Wang, B.; Li, B.; Xiong, J.; Li, C. Y. *Macromolecules* **2008**, *41*, 9516.
(33) Yoshioka, T.; Dersch, R.; Tsuji, M.; Schaper, A. K. *Polymer* **2010**, *51*, 2383.
(34) Chen, X.; Dong, B.; Wang, B.; Shah, R.; Li, C. Y. *Macromolecules* **2010**, *43*, 9918.
(35) Xu, H.; Xie, L.; Chen, Y.; Huang, H.; Xu, J.; Zhong, G. *ACS Sustainable Chem. Eng.* **2013**, DOI: 10.1021/sc4003032.
(36) Xu, X.; Jiang, L.; Zhou, Z.; Wu, X.; Wang, Y. *ACS Appl. Mater. Interfaces* **2012**, *4*, 4331.
(37) Bai, H.; Deng, H.; Zhang, Q.; Wang, K.; Fu, Q.; Zhang, Z.; Men, Y. *Polym. Int.* **2012**, *61*, 252.
(38) Somani, R. H.; Yang, L.; Sics, I.; Hsiao, B. S.; Pogodina, N.; Winter, H. H.; Agarwal, P.; Fruitwala, H.; Tsou, A. *Macromol. Symp.* **2002**, *185*, 105.
(39) Ten, E.; Jiang, L.; Wolcott, M. P. *Carbohyd. Polym.* **2012**, *90*, 541.
(40) Liu, L. Q.; Tasis, D.; Prato, M.; Wagner, H. D. *Adv. Mater.* **2007**, *19*, 1228.
(41) Ye, H.; Lam, H.; Titchenal, N.; Gogotsi, Y.; Ko, F. *Appl. Phys. Lett.* **2004**, *85*, 1775.
(42) Sui, X.; Wagner, H. D. *Nano Lett.* **2009**, *9*, 1423.
(43) Pai, C. L.; Boyce, M. C.; Rutledge, G. C. *Polymer* **2011**, *52*, 6126.
(44) Young, R. J.; Lovell, P. A. *Introduction to Polymers*; CRC Press: Boca Raton, FL, 2011.
(45) Agarwal, B. D.; Broutman, L. J.; Chandrashekhara, K. *Analysis and performance of fiber composites*; John Wiley & Sons, Inc.: Hoboken, NJ, 2006.